

Supplementary Material

Electrospinning Perylene Dianhydride Electrodes with Fine Micro-Nanostructures for High-Performance Lithium-Organic Batteries

Xi Liu,*^a Zhiling He,^a Junfeng Zhu,^a Jiru Jia,*^b Deyi Liao,^a Yichao Yang^a Longfei Fan,^a Chan Zhang,^a Runfeng Xiao^a and Shaobo Han*^a

^aSchool of Textile Materials and Engineering, Wuyi University, Jiangmen 529020, China.

^bSchool of Textile Garment and Design, Changshu Institute of Technology, Suzhou 215500, China.

*Corresponding author.

E-mail address: liuxi@wyu.edu.cn (X. L.); jiru.jia@cslg.edu.cn (J. J.); hanshaobo@wyu.edu.cn (S. H.)

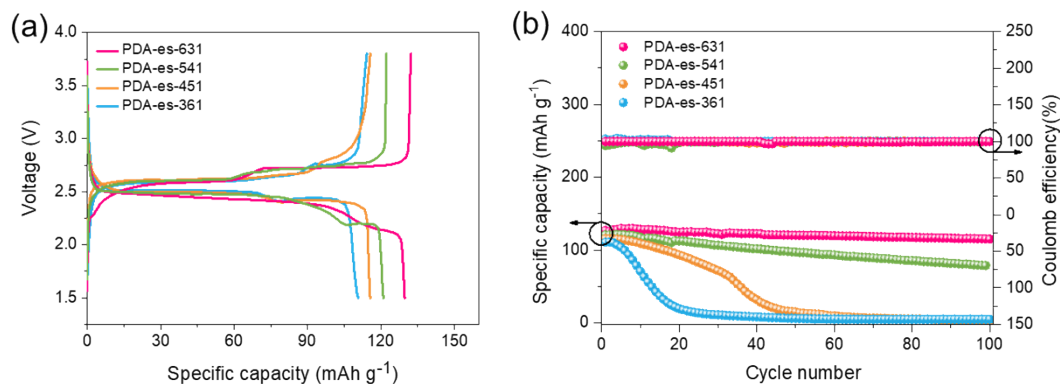


Fig. S1. (a) Discharge/charge profiles of the different ratios (PDA-es-631, PDA-es-541, PDA-es-451, and PDA-es-361)-based batteries in first cycles at 10 mA g⁻¹; (b) Cycling performance and Coulombic efficiency of the batteries under a current rate of 100 mA g⁻¹.

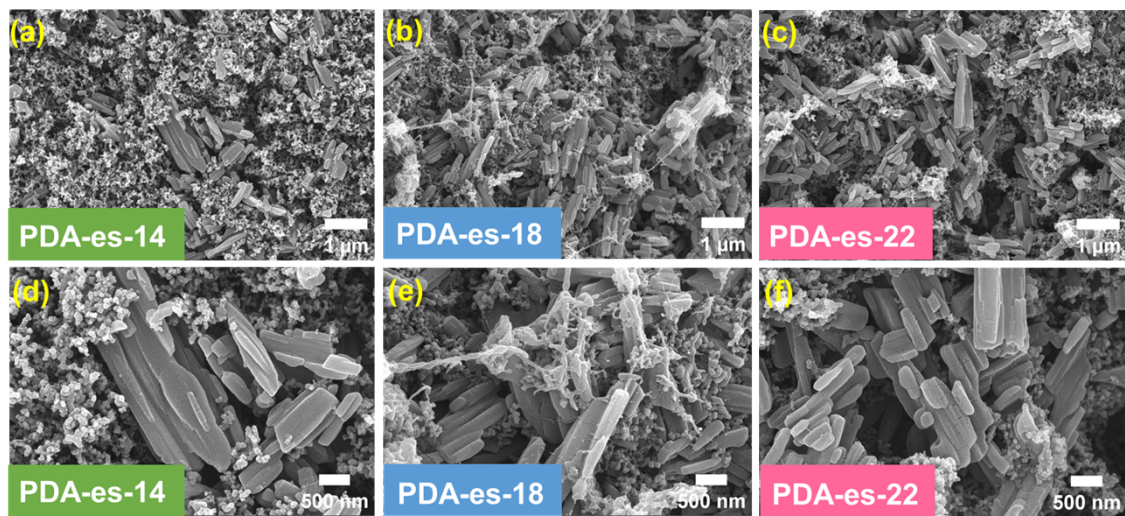


Fig. S2. SEM images of PDA-es-14, PDA-es-18, and PDA-es-22 electrodes.

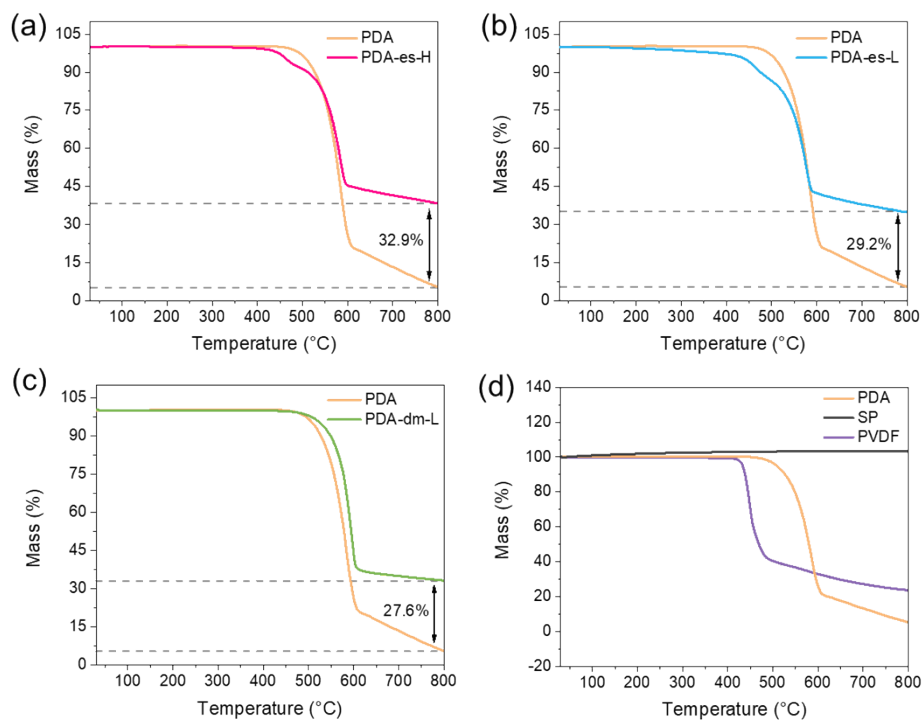


Fig. S3. TG curves of the corresponding compounds.

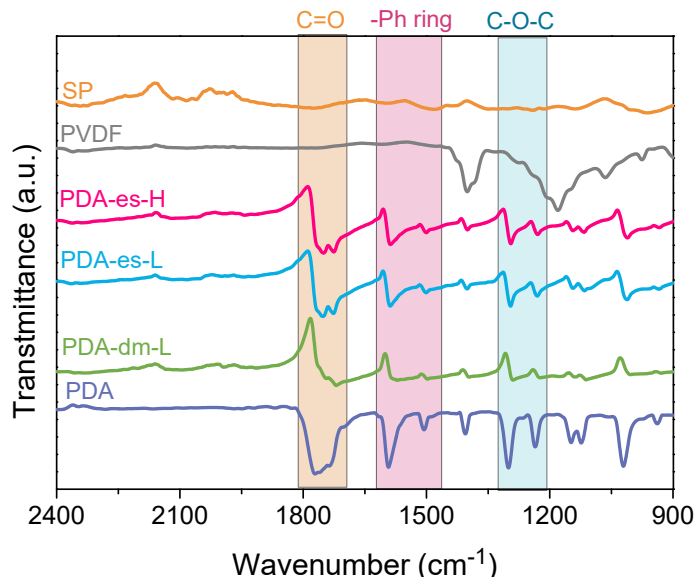


Fig. S4. FTIR results of PDA, PVDF, and SP powders and PDA-es-H, PDA-es-L, and PDA-dm-L electrodes.

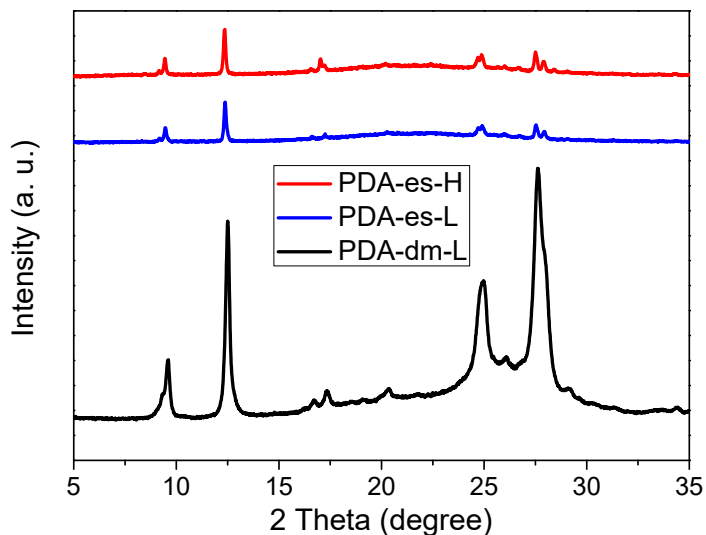


Fig. S5. XRD patterns of PDA-es-H, PDA-es-L, and PDA-dm-L electrodes.

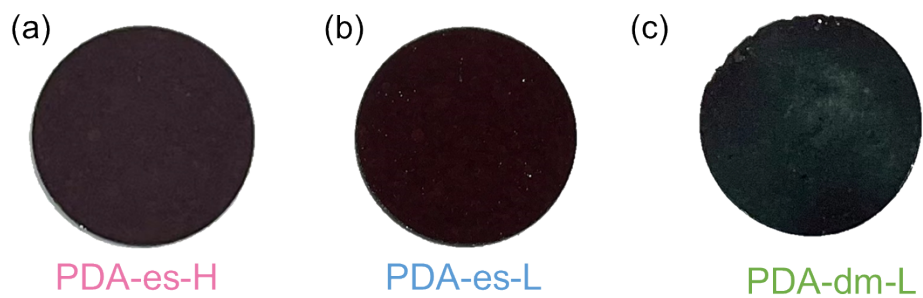


Fig. S6. Digital photographs of the three electrodes. The diameter of all these electrodes was 1.2 cm.

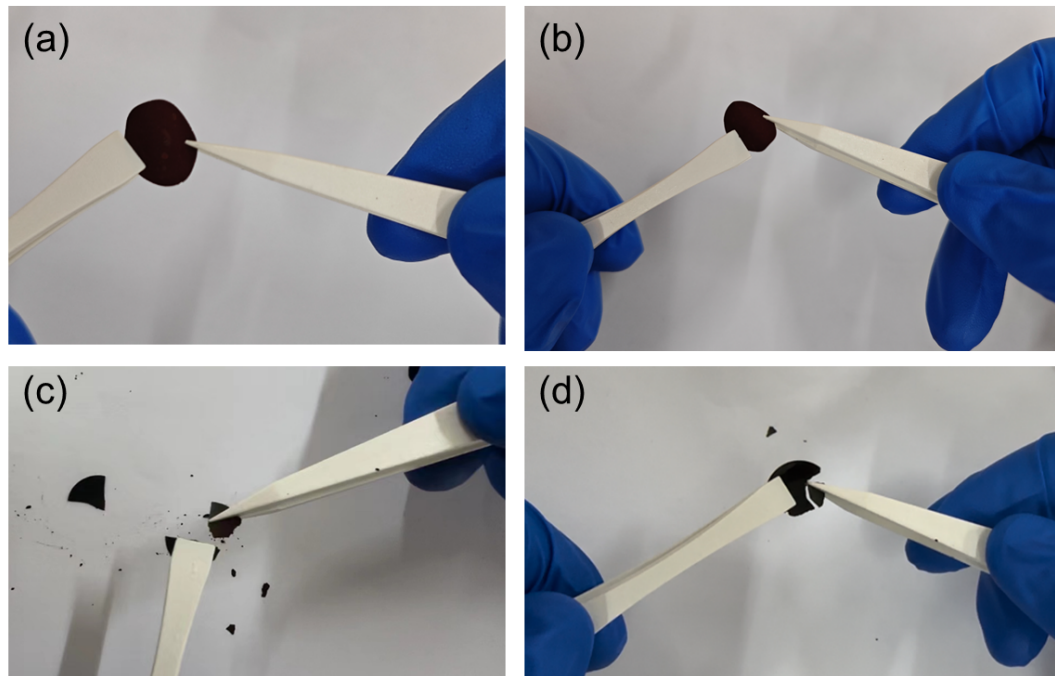


Fig. S7. The bending test digital photographs of PDA-es-H (a), PDA-es-L (b), PDA-dm-L (c), and PDA-dm-H (d) electrodes. The diameter of all these electrodes was 1.2 cm.

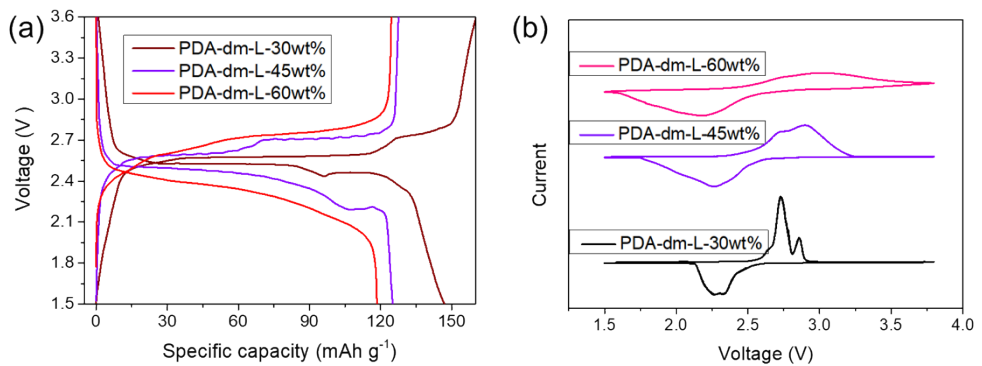


Fig. S8. Discharge/charge profiles (a) and CV curves (b) of 30wt%, 45wt%, and 60wt% PDA loaded dry-mixed electrodes.

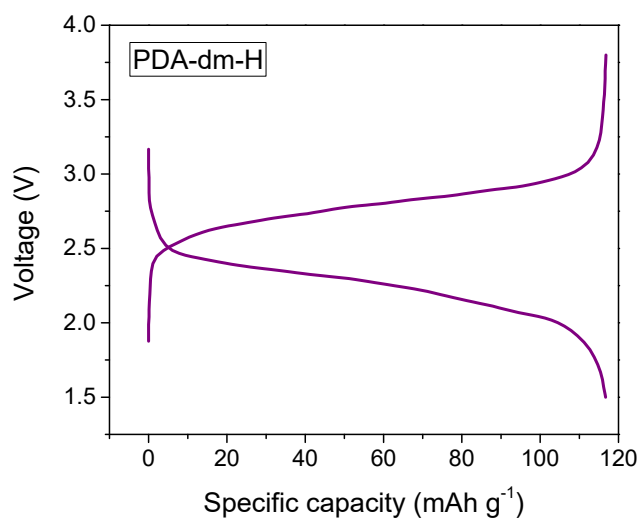


Fig. S9. Discharge/charge profiles of PDA-dm-H-based battery in first cycles at 10 mA g^{-1} .

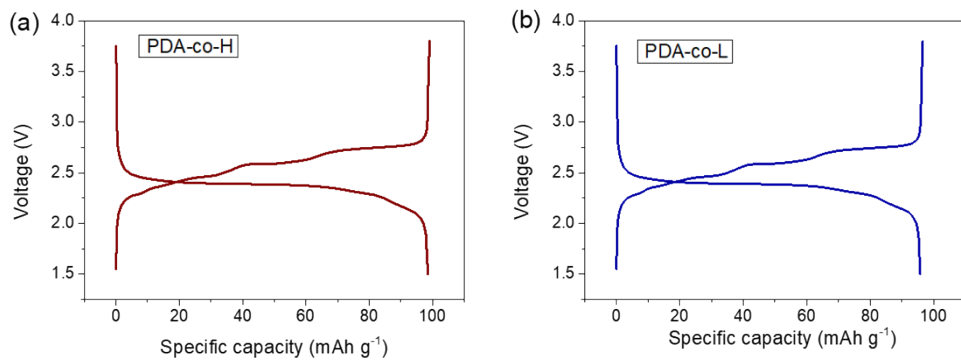


Fig. S10. Discharge/charge profiles of the coated electrodes-based batteries, PDA-co-H (a) and PDA-co-L (b), in first cycles at 10 mA g^{-1} .

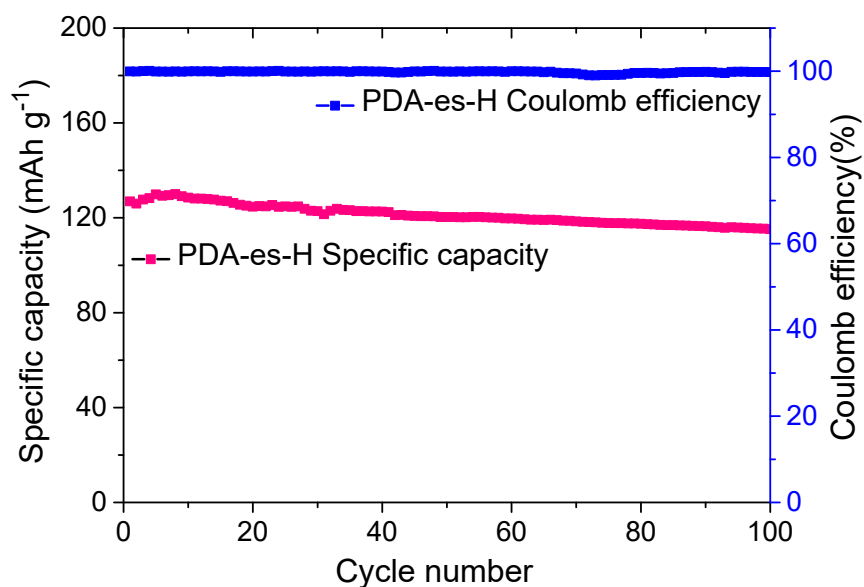


Fig. S11. Cycling performance and Coulombic efficiency of PDA-es-H battery under a current rate of 50 mA g^{-1} .

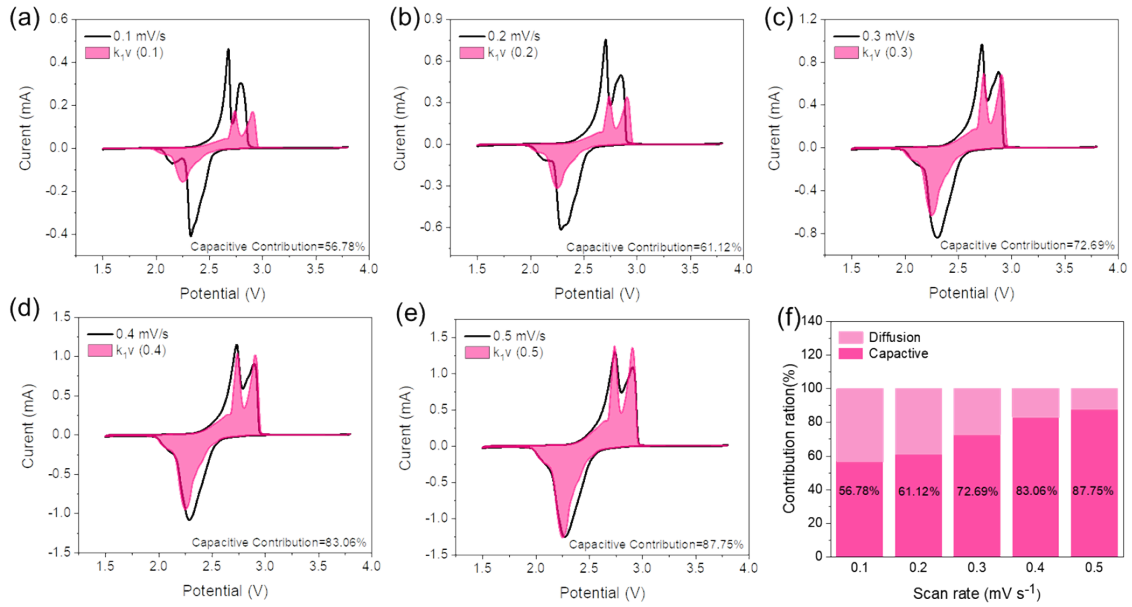


Fig. S12. CV curves and capacitive contributions of PDA-es-H electrode at scan rates of (a) 0.1, (b) 0.2, (c) 0.3, (d) 0.4, and (e) 0.5 mV s^{-1} ; (f) capacity contribution ratios of diffusion control and surface control at different scan rates.

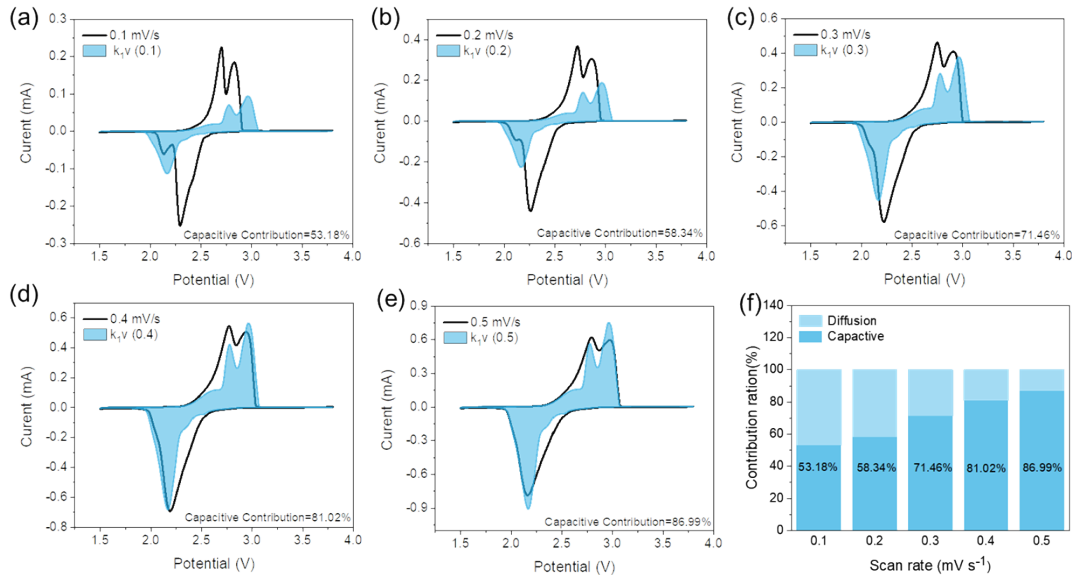


Fig. S13. CV curves and capacitive contributions of PDA-es-L electrode at scan rates of (a) 0.1, (b) 0.2, (c) 0.3, (d) 0.4, and (e) 0.5 mV s^{-1} ; (f) capacity contribution ratios of diffusion control and surface control at different scan rates.

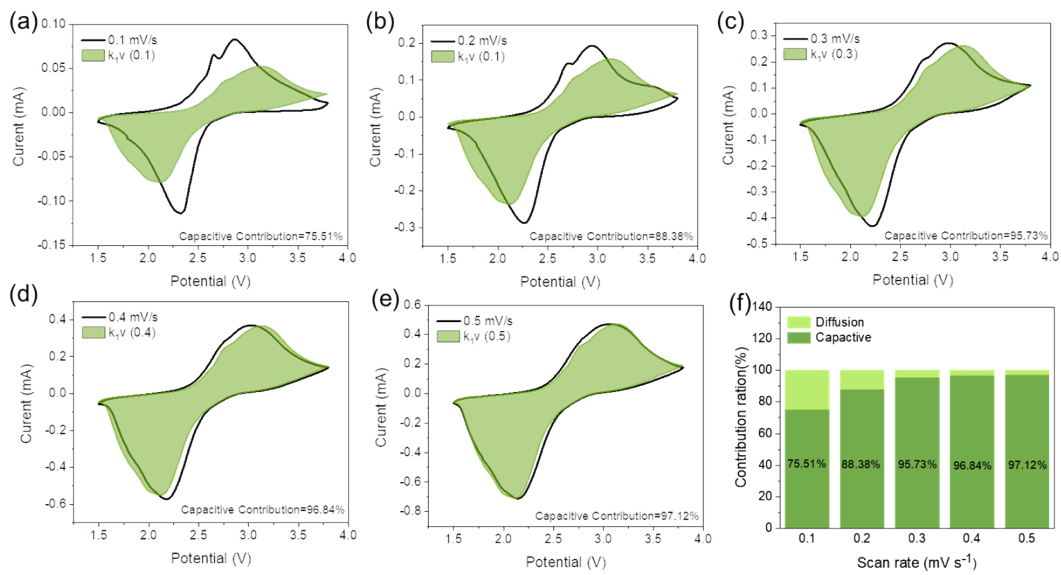


Fig. S14. CV curves and capacitive contributions of PDA-dm-L electrode at scan rates of (a) 0.1, (b) 0.2, (c) 0.3, (d) 0.4, and (e) 0.5 mV s⁻¹; (f) capacity contribution ratios of diffusion control and surface control at different scan rates.

Table S1. EA calculation results of the electrodes.

	Element content			Theoretical weight ratio	Actual weight ratio
	C [wt.%]	H [wt.%]	O [wt.%]	PDA [wt.%]	PDA [wt.%]
PDA-dm-L	77.25	1.63	15.87	60.88	64.81
PDA-es-H	77.39	1.81	15.01	60.42	61.29
PDA-es-L	76.81	1.78	15.39	60.67	62.84